Applied Surface Science 421 (2017) 240–246

Contents lists available at ScienceDirect

Applied Surface Science

journal homepage: www.elsevier.com/locate/apsusc

Full Length Article

Electrospinning, preparation and photoluminescence properties of $CoNb_2O_6$:Dy^{3+} incorporated polyamide 6 composite fibers

Ramazan Erdem[a,*], Mustafa İlhan[b], Mete Kaan Ekmekçi[c], Özlem Erdem[d]

[a] Textile Technology Department, Serik G.-S. Sural Vocational School of Higher Education, Akdeniz University, 07500, Serik, Antalya, Turkey
[b] Department of Metallurgical and Materials Engineering, Marmara University, Göztepe Kampüsü, Kadıköy, 34722, İstanbul, Turkey
[c] Department of Chemistry, Marmara University, Göztepe Kampüsü, Kadıköy, 34722, İstanbul, Turkey
[d] Textile Technology Department, Adana Vocational School of Higher Education, Cukurova University, 01160, Adana, Turkey

ARTICLE INFO

Article history:
Received 22 September 2016
Received in revised form
14 November 2016
Accepted 18 November 2016
Available online 22 November 2016

Keywords:
Electrospinning
Composite fiber
Columbite $CoNb_2O_6$
Optical properties
XRD
SEM-EDS

ABSTRACT

3 mol% Dy^{3+} doped cobalt niobate ($CoNb_2O_6$) compound has been synthesized by molten salt method using Li_2SO_4/Na_2SO_4 salt mixture as a flux at a relatively low temperature as compared to solid state reaction. X-ray diffraction patterns of 3 mol% Dy^{3+} doped $CoNb_2O_6$ compound indicated orthorhombic columbite single phase. SEM analysis revealed that Dy^{3+} doped $CoNb_2O_6$ has a submicron particle size. The photoluminescence of $CoNb_2O_6$:Dy^{3+} phosphor has exhibited in a dominant yellow emission at 579 nm with an excitation wavelength of 366 nm. The synthesized submicron phosphor particles were successfully incorporated into Polyamide 6 fibers by utilizing electrospinning technique. The average fiber diameter obtained through the process ranged between 192 ± 62 nm and 387 ± 341 nm. Mechanical characteristics of the produced nanofibrous webs were strongly influenced by the fiber morphologies and size (diameter) distribution rather than the phosphor particles incorporated into the fibers and/or located on the web. The photoluminescence of composite fiber material increased with the increasing phosphor content.

© 2016 Elsevier B.V. All rights reserved.

1. Introduction

In order to develop new useful technologies in different areas such as lighting, medical, military, laser applications, high energy photoluminescent and cathodoluminescent flat panel displays, holography and entertainment industry have required a search for smart functional materials and innovative synthesis methods to improve the performance and functionality of phosphors. The trivalent rare earth (RE) ions (Eu^{3+}, Dy^{3+}, Ho^{3+} etc.) doped materials have attracted a remarkable interest recently, due to their photoemission throughout the visible and infrared spectral range. The bright luminescence of these materials enable a new generation of lighting and display devices to be utilized safely with good thermal and chemical stability [1,2]. RE^{3+} activated oxide phosphors exhibit luminescence arising from the $3d \rightarrow 3d$, $5d \rightarrow 4f$ or $4f \rightarrow 4f$ transitions. The performance of optical materials require high purity, single phase and reduced particle size with uniform composition for the new flat panel display developments [3–5]. Moreover, in recent years, white light emitting diodes (W-LEDs) have been considered as next generation solid state lighting sources due to the advantages of long lifetime, energy saving, high efficiency, reliability and environmentally friendly properties [6]. Trivalent dysprosium (Dy^{3+}) ion has two typical band transitions in the 4f-4f emission spectrum as the yellow band around 570–590 nm due to $^4F_{9/2} \rightarrow {}^6H_{13/2}$ transition and the blue band about 475–495 nm due to $^4F_{9/2} \rightarrow {}^6H_{15/2}$ transition [5,6].

Among the cobalt niobates, $CoNb_2O_6$ crystallizes in both columbite (orthorhombic) and trirutil (tetragonal) structures. $CoNb_2O_6$ crystal possesses a low-symmetry crystal structure and the Co and Nb cations are at the centre of the octahedral surrounded by six oxygen atoms by sharing edges and forming chains along the b-axis in the $CoNb_2O_6$ orthorhombic columbite structure as seen from Fig. 1 [7,8]. $CoNb_2O_6$ is a good candidate being as a coating material for mechanical filters which are used for resonators and capacitors [9,10]. $CoNb_2O_6$ exhibits the quasi-one-dimensional Ising magnetic properties at 2.95 K [11]. The gas sensing behavior of $CoNb_2O_6$ was investigated by Balamurugan et al. [12]. $CoNb_2O_6$ is well known compound for the preparation of single phase perovskite $Pb(Co_{1/3}Nb_{2/3})O_3$, which have importance for multilayer ceramic capacitor, transducer, electrostrictor and actuator applications [13,14]. $CoNb_2O_6$ was also reported to be a potential microwave dielectric resonator material [15–17].

* Corresponding author.
E-mail address: ramazanerdem@akdeniz.edu.tr (R. Erdem).

http://dx.doi.org/10.1016/j.apsusc.2016.11.134
0169-4332/© 2016 Elsevier B.V. All rights reserved.

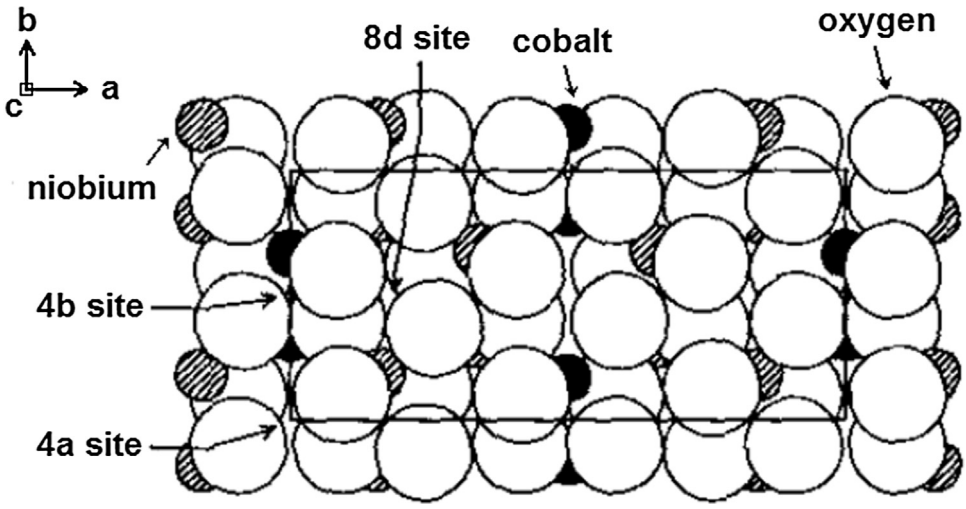

Fig. 1. Schematic illustration of the crystal structure of $CoNb_2O_6$ along the c axis.

Several different synthesis techniques have been used to prepare $CoNb_2O_6$, such as solid state synthesis [18], co-precipitation [19] and hydrothermal [20] methods in the literature. On the other hand, molten salt route provides lower calcination temperature and heat treatment time than that of the conventional solid state method to prepare $CoNb_2O_6$. Besides, molten salt synthesis helps to provide high homogeneity, single phase formation, and a small particle size in one-step reaction [21,22]. In addition, molten salt or salt mixtures can be easily removed from the main compound by washing with distilled water after the synthesis reaction [23–25]. Molten salt synthesis method has been rarely reported for the preparation of undoped and RE ion doped $CoNb_2O_6$ in the literature [26].

In order to increase the thermal and mechanical properties as well as to enhance the usage area, RE complexes could be incorporated into the polymer fibers. It has been proven that the RE complexes doped polymer matrix materials have excellent luminescence property and smooth surface [27]. Within this direction, electrospinning is a suitable method to prepare 1D nanostructure easily from organic-inorganic materials. This typical electrostatic process includes several operational steps: (i) charging of the fluid, (ii) formation of the cone-jet, (iii) thinning of the instable jet in an electric field and (iv) collection of the fibers on a suitable collector. It is commonly accepted that the diameter and morphology of the electrospun fibers are strongly dependent on the solution properties (viscosity, conductivity, molecular weight, surface tension, polymer concentration and solvent type), process parameters (applied electric field, tip to collector distance and feeding rate) and ambient conditions (humidity and temperature of the surroundings) [28–31]. There are several investigations on the luminescent properties of electrospun fiber composite materials. For example, Poly(vinyl alcohol)/$[EuW_{10}O_{36}]_9$ composite fibers were obtained by the electrospinning technique [32]. In this case, no phase separation was observed and the resulting composite material was highly luminescent. Luminescent composite fibers of poly(vinyl pyrrolidone) (PVP) and Y_2O_3/Eu^{3+} nanocrystals were prepared by electrospinning. The composite fibers were in a random orientation, with an average diameter of about 300 nm and length up to several tens of micrometers [33]. The Ln^{3+} doped $NaYF_4$/poly(vinyl pyrrolidone) (PVP) nanocomposite fibers with an average diameter of 300–800 nm were prepared by electrospinning. The $NaYF_4$ nanoparticles have the size between 5 and 20 nm. Upon laser excitation at 980 nm, blue up conversion emission was observed for the PVP-dispersed $NaYF_4$ nanoparticles co-doped with $Yb^{3+}$and Tm^{3+}. White light with more stable color balance (blue of Tm^{3+}, green and red of Er^{3+}) was obtained for the triply doped $NaYF_4/(Yb^{3+},Tm^{3+},Er^{3+})$ nanoparticles [34].

In this paper, 3 mol% Dy^{3+} doped $CoNb_2O_6$ was synthesized by molten salt synthesis and then incorporated into Polyamide 6 fibers by using electrospinning technique. The reason for choosing 3 mol% Dy^{3+} doping concentration is due to investigation on the luminescence properties of Dy^{3+} doped $CoNb_2O_6$ phosphors previously studied by Ekmekçi et al. [35]. Spectral characterization of $CoNb_2O_6$:Dy^{3+} phosphor and composite fibers in UV–vis spectral region has been performed. The morphology of $CoNb_2O_6$:Dy^{3+} phosphor particles incorporated on the electrospun fibers was also studied by SEM-EDS analyses. To our knowledge this is the first report on the $CoNb_2O_6$:Dy^{3+} incorporated composite fibers obtained by applying both molten salt synthesis and electrospinning technique.

2. Materials and method

2.1. Molten salt synthesis of the powders

Dy^{3+} doped $CoNb_2O_6$ and undoped $CoNb_2O_6$ for comparing were synthesized via molten salt route by mixing starting materials of cobalt nitrate $[Co(NO_3)_2{\cdot}6H_2O]$ and niobium oxide (Nb_2O_5) at a salt to oxide weight ratio of 2:1. Li_2SO_4-Na_2SO_4 salt mixture was used as flux at molar ratio of 0.635/0.365. After mixing of starting materials (cobalt nitrate, niobium oxide, and dysprosium oxide) in an agate mortar, Li_2SO_4 and Na_2SO_4 salt mixture was subsequently added into the first mixture and ground well for the last time to provide homogeneity. After the calcination of sufficient amount of powder mixture at 800 °C for 4 h in an alumina crucible, they were washed with ultrapure water and vacuum filtered several times in order to remove ionic salts from the resultant niobate compound. The presence of the sulfate ions in filtrate were controlled by qualitative reactions.

2.2. Preparation and characterization of the polymer solution

PA6 (17 wt.%) was dissolved in Formic Acid (FA) by laboratory type magnetic stirrer (Stuart, SB 162) at 60 °C for 6 h. Three separate solutions were prepared and the total mass of each solution was 10 g. Then, 0.05 g, 0.1 g and 0.2 g $CoNb_2O_6$:Dy^{3+} phosphor particles were added into the PA6 solution subsequently and stirred another 2 h. In order to obtain homogenized dispersed medium, the blend solution was kept in ultrasound bath (Alexandra Ultrasonic

Cleaner) for half an hour (220 V/50–60 Hz) before electrospinning. Viscosities of the solutions were identified with Brookfield Digital Viscosimeter by using s21 type spindle with the rotational speed of 50 rpm/min. The electrical conductivity of the solutions was also measured with a laboratory type conductivity meter (WTW, Cond3110) under ambient atmosphere.

2.3. Electrospinning process

Electrospinning was performed in the laboratory spinning unit (NS24, NanoFMG) in vertical alignment (bottom-up spinning). Each solution was placed in a 10 ml syringe and only 1 ml was sent to the stationary ground cylindrical drum collector (covered with a piece of aluminum foil) through a 20 gauge nozzle. The power supply (AC) was set up for a positive voltage of 34.6–38 kV. The flow rate of the solution was also determined by setting up the syringe pump between 0.10–0.15 ml/h. The rotational speed of the drum collector was 35 rpm/min and its distance was set to 15–15.5 cm (optimum distance based on preliminary tests) away from the nozzle. At the time of the experiments, relative humidity and temperature values ranged from 52 to 62% RH and 24–28 °C.

2.4. Structural and optical characterization of sintered powders and electrospun composite fibers

The phase determination of sintered powders were investigated by X-ray diffractometer (XRD, Rigaku Corp., D-MAX 2200) using Cu-K_α radiation at a scan rate of 2°/min between 20−−65° and Ni filter. The surface morphology and elemental composition of sintered powders and $CoNb_2O_6$:Dy^{3+} incorporated electrospun fibers were performed by scanning electron microscopy (SEM; Jeol JSM 5910LV) equipped with energy dispersive spectroscopy (EDS; Oxford Instruments Inca X-Sight 7274). Photoluminescence (PL) measurements were recorded by using a Scinco floromaster-FS/2 model fluorometer with a Xe-arc lamp (150 W) as excitation source. All of the measurements were carried out at room temperature.

2.5. Mechanical properties of electrospun fibers

In order to determine the mechanical properties (tensile strength and elongation) of the pristine PA6 fibrous web and $CoNb_2O_6$:Dy^{3+} incorporated composite fibrous webs, tensile and recovery tests were performed by using an Instron Machine (Instron4411) at ambient environment (22 ± 3 °C temperature and 50 ± 5% relative humidity). The samples were cut into approximately 30 mm × 10 mm (length × width) in both machine and transverse directions in order to be placed conveniently into the uniaxial testing machine. During the experiment, 50 N load cells under a cross-head speed of 10 mm/min were applied to the specimens. Three repetitions were taken for each specimen in order to measure average tensile strength and elongation at break values.

3. Results and discussion

3.1. X-ray diffraction and SEM-EDS characterization of undoped $CoNb_2O_6$ and 3 mol% Dy^{3+} doped $CoNb_2O_6$

Fig. 2 shows the XRD results of 3 mol% Dy^{3+} doped $CoNb_2O_6$ and undoped $CoNb_2O_6$ were synthesized by using the molten salt route. XRD analysis revealed Dy^{3+} doped $CoNb_2O_6$ identical with undoped $CoNb_2O_6$ single phase that crystallized (JCPDS card no: 32-0304) in orthorhombic symmetry with space group *Pbcn*(60) having the columbite type structure. As seen from Fig. 1, there are three kinds of empty octahedral sites as 4*a*, 4*b* and 8*d* in the columbite structure [36] in which the ion's radius and CN (coordination number) of Co^{+2} (CoO_6) and Nb^{+5} (NbO_6) are 0.65 Å (for 6C.N) and 0.64 Å (for 6C.N) respectively. Among the octahedral (4*a*, 4*b*, 8*d*) sites, when Dy^{3+} ions insert into 8*d* sites, this may lead to a large repulsive force on adjacent Nb^{5+} ions. On the other hand, the 4*b* sites are compressed due to the Jahn-Teller distortion of adjacent CoO_6 octahedral, while the 4*a* sites are relatively free. The 4*b* sites deformation would become relaxed if the Jahn-Teller Co^{2+} cations disappear. Hence, based on the ion's radius and valence, the Dy^{3+} ions having an ionic radius of 0.912 Å (for 6C.N) might occupy firstly 4*a* and then 4*b* sites up to 3 mol% doped concentration [36].

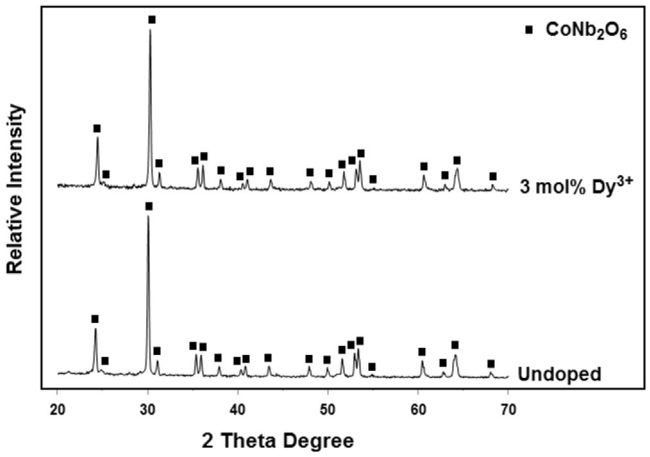

Fig. 2. X-ray diffraction patterns of undoped and Dy^{3+} doped $CoNb_2O_6$ structures.

Fig. 3(a–b) shows the SEM micrographs (at 5.000 × magnification) and EDS spectra of undoped $CoNb_2O_6$ and 3 mol% Dy^{3+} doped $CoNb_2O_6$. SEM analysis showed that the grain size of $CoNb_2O_6$ decreased for 3 mol% Dy^{3+} doped $CoNb_2O_6$ sample compared with the undoped one. The structures of undoped and Dy^{3+} doped $CoNb_2O_6$ particles exhibited oval like shapes and submicron grain sizes varied between approximately 0.2 and 0.8 μm. EDS analysis revealed that the weight and atomic elemental compositions of undoped $CoNb_2O_6$ and Dy^{3+} doped $CoNb_2O_6$ were in agreement with their theoretical compositions.

3.2. Solution properties and fiber morphologies

Successful and continuous electrospinning process was performed for each prepared solutions. Table 1 illustrates the details of solution properties, process parameters and related nanofiber diameters of electrospun nanofibers. According to Table 1, viscosity of the solutions increased with the content of $CoNb_2O_6$:Dy^{3+} particles increased in the solution. On the other hand, it was noticed that the electrical conductivity of the solutions tend to decrease with increasing content of the particles in the solution.

The morphologies of the electrospun nanofibers were investigated by SEM analysis (at 5.000 × magnification). Fig. 4(a–d) displays that uniform and defect free fibers, with average diameters ranging from 192 nm to 387 nm, were obtained from all of the prepared solutions. Also, it was found that $CoNb_2O_6$:Dy^{3+} phosphor particles were well dispersed on the fibrous webs. SEM-EDS analyses have been performed in order to determine phosphor particles on the fibrous webs. EDS spectrum of 0.2 g $CoNb_2O_6$:Dy^{3+} incorporated PA6 sample were given in Fig. 5. The elemental composition was detected by EDS analysis at 20 kV of SEM acceleration voltage and an area scanning at 5000× magnification. As it is seen from EDS spectrum, Co/Nb atomic ratio and presence of Dy^{3+} are indicated to $CoNb_2O_6$:Dy^{3+} structure.

The smallest fiber diameter (192 ± 62 nm) was gained from the solution including 0.1 g $CoNb_2O_6$:Dy^{3+} particles with applied voltage of 38 kV at 15.5 cm distance. This implies that applied voltage

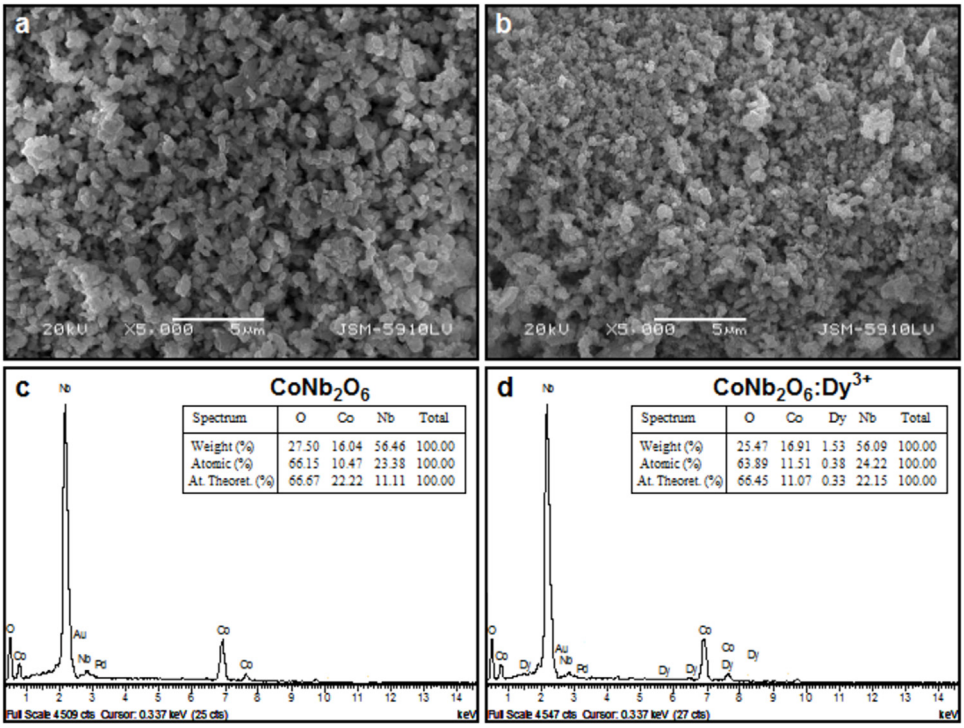

Fig. 3. SEM micrographs of (a) undoped and (b) 3 mol%, Dy^{3+}doped $CoNb_2O_6$ at 5.000 × magnification, EDS spectra of (c) undoped and (d) 3 mol%, Dy^{3+}doped $CoNb_2O_6$.

Table 1
Solution properties and process parameters of Pristine PA 6 and $CoNb_2O_6$:Dy^{3+} incorporated composite fibers.

	Solution properties		Process parameters			
Polymers	Viscosity (cP)	Conductivty (mS/cm)	Feeding rate (ml/h)	Applied voltage (kV)	Distance (cm)	Fiber diameter (nm)
Pristine PA 6	486	4.72	0.15	34.6	15	266 ± 150
0.05 g $CoNb_2O_6$:Dy^{3+} Inc. PA 6	503	4.66	0.10	35	15.5	387 ± 341
0.1 g $CoNb_2O_6$:Dy^{3+} Inc. PA 6	530	4.61	0.10	38	15.5	192 ± 62
0.2 g $CoNb_2O_6$:Dy^{3+} Inc. PA 6	538	4.54	0.15	35	15.5	293 ± 197

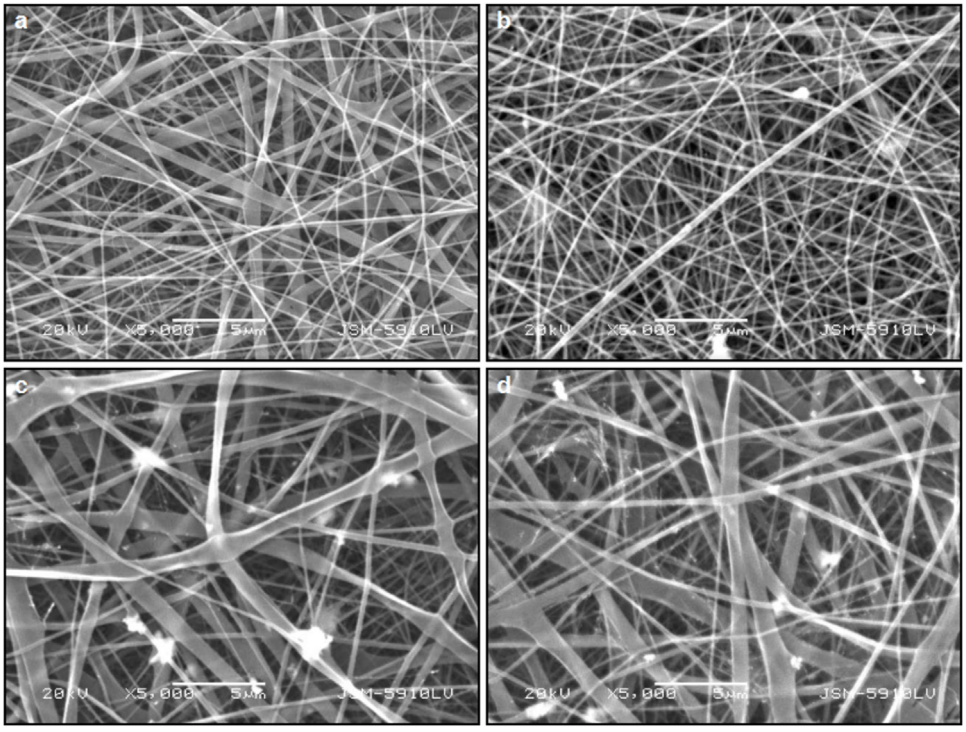

Fig. 4. SEM micrographs of (a) pristine PA 6 fibers and (b) 0.05 g, (c) 0.10 g, (d) 0.2 g of $CoNb_2O_6$:Dy^{3+}incorporated composite fibers at magnification 5.000×.

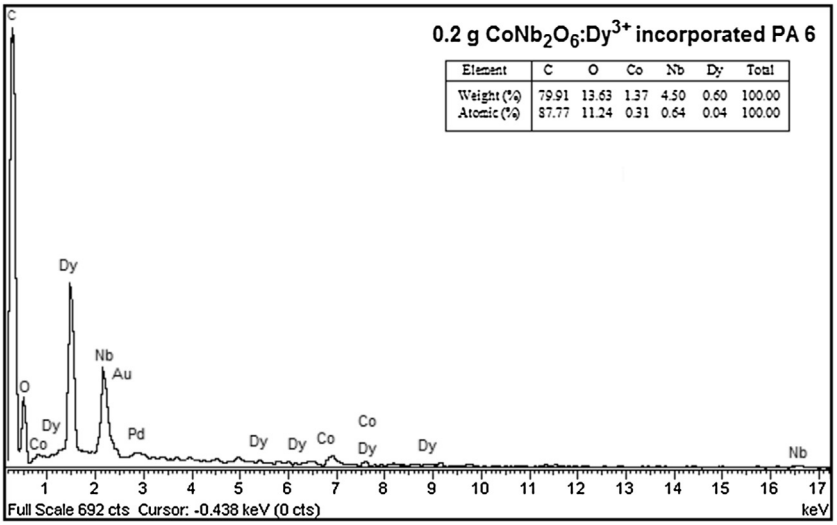

Fig. 5. EDS spectrum of 0.2 g $CoNb_2O_6$:Dy^{3+} incorporated composite fibers.

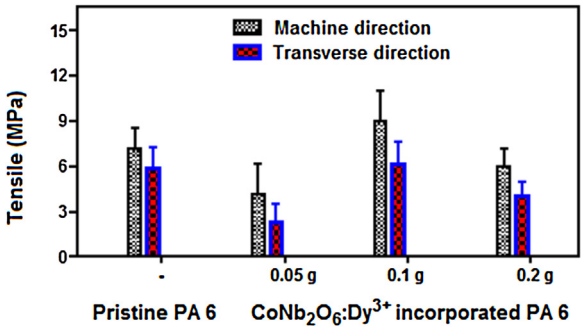

Fig. 6. The tensile properties of pristine PA 6 and $CoNb_2O_6$:Dy^{3+} incorporated composite PA 6 fibers.

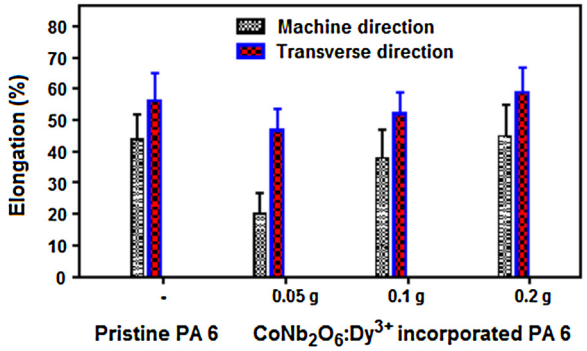

Fig. 7. The elongation properties of pristine PA 6 and $CoNb_2O_6$:Dy^{3+} incorporated composite PA 6 fibers.

was very critical to determine the fiber diameter in our case which is consistent with the literature [37]. It can also be speculated that the range between the finest and the coarsest fiber diameters in each sample was dramatically widened, and this gap elevated remarkably for the fibers containing 0.05 g and 0.2 g $CoNb_2O_6$:Dy^{3+} particles. This situation may be explained by some amount of the precipitated $CoNb_2O_6$:Dy^{3+} particles at the edge of the nozzle during the process which influenced negatively the regular feeding of the solution into the electrical field. Again, increasing applied voltage encouraged smooth and stable electrospinning and prevented undesired precipitation at the edge of the nozzle to the certain extent. Therefore, more coherent fiber diameter distribution was procured for the samples containing 0.1 g $CoNb_2O_6$:Dy^{3+} particles.

3.3. Mechanical properties of the electrospun nanofibrous webs

Figs. 6 and 7 exhibit the tensile and elongation test results of electrospun pristine and $CoNb_2O_6$:Dy^{3+} incorporated PA6 composite nanofibrous webs respectively. Findings revealed that the mechanical properties of the structures were highly correlated with the fiber characteristics and also fiber size (diameter) distribution. Because, when a specific force applied to the nanofibrous web, this force is distributed to the fibers constructed in the web [38]. Therefore, shape, morphology, diameter and uniformity of the fibers as well as the structural characteristics (porosity, number of fibers laid in per unit area et.) of the nanofibrous web determine the final mechanical property. According to the tensile graph, the greatest value (8.9 ± 1.9 MPa) was obtained in the machine direction for the composite fibrous web incorporated with 0.1 g $CoNb_2O_6$:Dy^{3+} where average fiber diameter (192 nm) and the size distribution (32.2%) were the smallest. On the other hand, the worst tensile result (2.3 ± 1.2 MPa) was gained in the transverse direction for the sample including 0.05 g $CoNb_2O_6$:Dy^{3+} where average fiber diameter (387 nm) and the size distribution (88.11%) were the largest. It was also observed that the tensile strength of the electrospun nanofibrous webs was noticeably higher in machine direction than in transverse direction. This is most probably associated with the fibers laid in more parallel in machine direction due to the rotating drum collector. On the other hand, elongation at break results of the nanofibrous webs varied irregularly. The greatest value ($59 \pm 8\%$) was obtained for 0.2 g $CoNb_2O_6$:Dy^{3+} incorporated PA6 composite nanofibrous web in the transverse direction, while the lowest result ($20 \pm 7\%$) was yielded for 0.05 g $CoNb_2O_6$:Dy^{3+} incorporated one in the machine direction. In conclusion, it can be claimed that $CoNb_2O_6$:Dy^{3+} phosphor particles, incorporated into the fibers and/or located onto the web, did not have much influence to the mechanical properties, instead, fiber characteristics and randomized distribution of the fibers had strong impact on the tensile and elongation results of the nanofibrous webs.

3.4. Optical characterization of $CoNb_2O_6$:Dy^{3+} incorporated electrospun nanofibrous webs

Fig. 8 shows the excitation spectra of $CoNb_2O_6$:Dy^{3+} (a: 0.05 g, b: 0.1 g, c: 0.2 g) incorporated electrospun composite nanofibrous

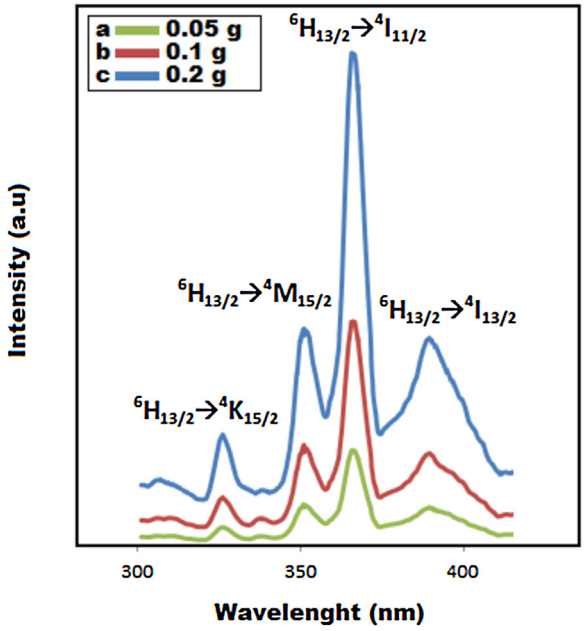

Fig. 8. Excitation spectra of $CoNb_2O_6$:Dy^{3+}incorporated composite fibers at λ_{em} = 579.

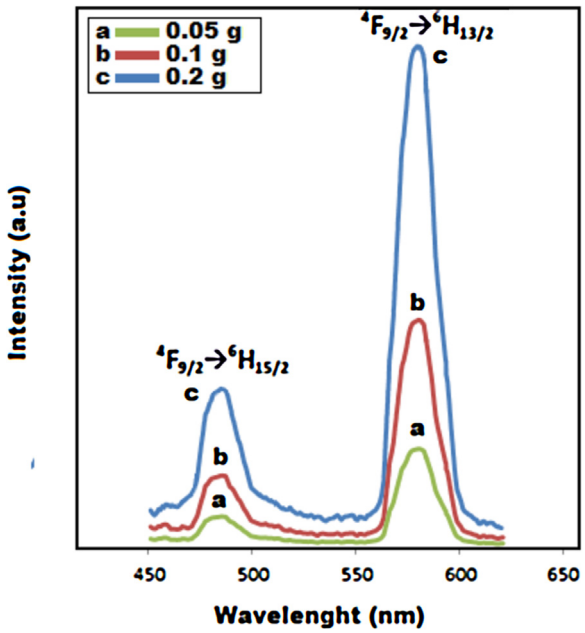

Fig. 9. Emission spectra of $CoNb_2O_6$:Dy^{3+} incorporated composite fibers at λ_{ex} = 366 nm.

webs with emission monitored at 579 nm. The excitation spectra in the 300–420 nm range belong to the transitions between the ground level $^6H_{13/2}$ and the excited levels $^4K_{15/2}$, $^4M_{15/2}$, $^4I_{11/2}$ and $^4I_{13/2}$ respectively. The assignments of the different excitation bands were identified on the basis of Dieke's energy level diagram [39]. The excitation spectra exhibited four excitation bands which were observed at $^6H_{13/2} \rightarrow {}^4K_{15/2}$ (327 nm), $^6H_{13/2} \rightarrow {}^4M_{15/2}$ (354 nm), $^6H_{13/2} \rightarrow {}^4I_{11/2}$ (366 nm), and $^6H_{13/2} \rightarrow {}^4I_{13/2}$ (388 nm) transitions. Among these excitation bands, wavelength of 366 nm was chosen to analyze PL properties of $CoNb_2O_6$:Dy^{3+}. Fig. 9 shows the emission spectra of $CoNb_2O_6$:Dy^{3+} (a: 0.05 g, b: 0.1 g, c: 0.2 g) electrospun composite nanofibrous webs under the excitation of 366 nm. The emission spectra exhibited two emission bands at 485 nm (blue region) and 579 nm (yellow region). Blue and yellow regions are the characteristic emissions of Dy^{3+} attributed to the $^4F_{9/2} \rightarrow {}^6H_{15/2}$ and $^4F_{9/2} \rightarrow {}^6H_{13/2}$ transitions respectively. The optical analysis of 3 mol% Dy^{3+} doped $CoNb_2O_6$ phosphor particles incorporated into the electrospun nanofibrous webs showed that the emission intensity increased by increasing $CoNb_2O_6$:Dy^{3+} phosphor content. A remarkable yellow emission was observed for c: 0.2 g sample at the highest rate of incorporation.

4. Conclusions

3 mol% Dy^{3+} doped $CoNb_2O_6$ and undoped $CoNb_2O_6$ crystalline particles were successfully synthesized by molten salt synthesis method. XRD analysis showed that all the synthesized particles exhibited single phase with orthorhombic columbite structure. Electrospinning process was performed well and uniform and defect free nanofibers were manufactured. Some amount of $CoNb_2O_6$:Dy^{3+} particles were precipitated at the edge of the nozzle during the process that influenced negatively the regular feeding of the solution into the electrical field, therefore, homogeneity of the fibrous webs undesirably affected. Increasing applied voltage encouraged smooth and stable electrospinning and prohibited undesired precipitation at the edge of the nozzle to the certain level. Measurements proved that the mechanical properties of the structures were highly depended on the fiber characteristics and also fiber size (diameter) distribution. Photoluminescence of $CoNb_2O_6$:Dy^{3+} phosphor particles incorporated into the nanofibrous webs showed a blue emission at about 485 nm and a yellow emission at about 579 nm respectively. Emission intensity of the electrospun composite nanofibrous webs increased, depending on phosphor particle content. Based on the obtained results, it was concluded that the $CoNb_2O_6$:Dy^{3+} phosphor incorporated electrospun composite fiber could be a promising material for optical fiber applications and fiber coupled LEDs.

References

[1] W. Zhang, Y. Huang, H. Seo, Luminescence properties and efficient energy transfer in Ce^{3+} and Tb^{3+} co-doped $Mg_2La_3[SiO_4]_2[PO_4]O$ phosphor, Ceram. Int. 39 (2013) 4313–4319.
[2] M. İlhan, Synthesis, structure and photoluminescence properties of Ho^{3+} doped TTB-$BaTa_2O_6$ phosphors, Solid State Sci. 38 (2014) 160–168.
[3] L.L. Shi, Y.L. Cheng, S. Qiang, Spectroscopic properties, energy transfer and structural analysis of Sr_2CeO_4:M^+ and Sr_2CeO_4:Eu^{3+} M^+ (M^+ = Li^+, Na^+, K^+), J. Fluoresc. 21 (2011) 1461–1466.
[4] C.H. Yang, G.F. Yang, Y.X. Pan, Q.Y. Zhang, Synthesis and spectroscopic properties of $GdAl_3(BO_3)^4$ poly-crystals codoped with Yb^{3+} and Eu^{3+}, J. Fluoresc. 19 (2009) 105–109.
[5] K.N. Shinde, S.J. Dhoble, Luminescence in Dy^{3+} and Eu^{3+} activated $K_3Al_2(PO_4)_3$, J. Fluoresc. 21 (2011) 2053–2056.
[6] R.S. Ukare, V. Dubey, G.D. Zade, S.J. Dhoble, PL properties of Sr_2CeO_4 with Eu^{3+} and Dy^{3+} for solid state lighting prepared by precipitation method, J. Fluoresc. 26 (2016) 791–806.
[7] J.H. Strudivant, The crystal structure of columbite, Z. Kristallogr. 75 (1930) 88–108.
[8] V. Antonietti, E.J. Kinast, L.I. Zawislak, J.B.M. da Cunha, C.A. dos Santos, Structure refinement of mixed oxides $Fe_xCo_{1-x}Ta_2O_6$, J. Phys. Chem. Solids 62 (2001) 1239–1242.
[9] A.J. Moulson, J.M. Herbert, Electroceramics: Materials Properties Appications, Chapman and Hall, New York, 1990.
[10] A.S. Bhalla, R. Guo, R. Roy, The perovskite structure – a review of its role in ceramic science and technology, Mater. Res. Innov. 1 (2000) 3–26.
[11] S. Kobayashi, S. Mitsuda, T. Jogetsu, J. Miyamoto, H. Katagiri, K. Kohn, Anisotropic growth kinetics in the geometrically frustrated, Phys. Rev. B: Condens. Matter 60 (1999) 3331.
[12] C. Balamurugan, A.R. Maheswari, D.W. Lee, Structural optical, and selective ethanol sensing properties of p-type semiconducting $CoNb_2O_6$ nanopowder, Sens. Actuators B 205 (2014) 289–297.
[13] N. Vittayakorn, T. Tunkasiri, Dielectric properties and phase transition of polycrystalline lead zirconate titanate-lead cobalt niobate, Phys. Scr. 129 (2007) 199–204.
[14] T.R. Shrout, A. Halliyal, Preparation of lead-based ferroelectric relaxors for capacitors, Am. Ceram. Soc. Bull. 66 (1987) 704–711.

[15] S. Mitsuda, H. Okano, S. Kobayashi, K. Prokes, Non-magnetic impurity effect on domain growth kinetics in an isosceles triangular ising antiferromagnet $CoNb_2O_6$, J. Magn. Magn. Mater. E993 (2004) 272–276.
[16] R.C. Pullar, K. Okeneme, N. McN, Alford, Temperature compensated niobate microwave ceramics with the columbite structure $M^{2+}Nb_2O_6$, J. Eur. Ceram. Soc. 23 (2003) 2479–2483.
[17] V. Parvlescu, M. Ruwet, P. Grange, V.I. Parvlescu, Sol—gel synthesis of cobalt—niobia catalysts, Solid State Ionics 137 (1997) 101–103.
[18] N. Chaiyo, N. Vittayakorn, Effect of calcination conditions on phase formation of microwave dielectric cobalt niobate ($CoNb_2O_6$) powders via a mixed oxide synthesis route, J. Ceram. Process Res. 9 (2008) 381–384.
[19] I.S. Mulla, N. Natarajan, A.B. Gaikwad, V. Samuel, U.N. Guptha, V. Ravi, A coprecipitation technique to prepare $CoTa_2O_6$ and $CoNb_2O_6$, Mater. Lett 61 (2007) 2127–2129.
[20] R. Ma, F. Cao, J. Wang, G. Zhu, G. Pang, Hydrothermal synthesis and phase stability of $CoNb_2O_6$ with a rutile structure, Mater. Lett. 65 (2011) 2880–2882.
[21] K.H. Yoon, Y.S. Cho, D.H. Lee, D.H. Kang, Powder characteristics of $Pb(Mg_{1/3}Nb_{2/3})O_3$ prepared by molten salt synthesis, J. Am. Ceram. Soc. 76 (1993) 1373–1376.
[22] K.H. Yoon, Y.S. Cho, D.H. Kang, Molten salt synthesis of lead-based relaxors, J. Mater. Sci 33 (1998) 2977–2984.
[23] K.H. Yoon, Y.S. Cho, D.H. Lee, D.H. Kang, Powder characteristics of $Pb(Mg_{1/3}Nb_{2/3})O_3$ prepared by molten salt synthesis, J. Am. Ceram. Soc. 76 (1993) 1373–1376.
[24] K.H. Yoon, Y.S. Cho, D.H. Kang, Molten salt synthesis of lead-based relaxors, J. Mater. Sci. 33 (1998) 2977–2984.
[25] L. Guo, J. Dai, J. Tian, Z. Zhu, T. He, Molten salt synthesis of $ZnNb_2O_6$ powder, Mater. Res. Bull. 42 (2007) 2013–2016.
[26] M.K. Ekmekçi, M. Erdem, A.S. Başak, Molten salt synthesis, visible and near-IR region spectral properties of europium or neodymium doped $CoNb_2O_6$ columbite niobate, Dalton Trans. 44 (2015) 5379–5385.
[27] Q.L. Ma, W.S. Yu, X.T. Dong, J.X. Wang, G.X. Liu, J. Xu, J. Nanopart. Res. 14 (2012) 1–7.
[28] R. Erdem, İ. Usta, M. Akalın, O. Atak, M. Yüksek, A. Pars, The impact of solvent type and mixing ratios of solvents on the properties of polyurethane based electrospunnanofibers, Appl. Surf. Sci. 334 (2015) 227–230.
[29] R. Erdem, M. İlhan, E. Sancak, Analysis of EMSE and mechanical properties of sputter coated electrospun nanofibers, Appl. Surf. Sci. 380 (2016) 326–330.
[30] S. Budun, E. İşgören, R. Erdem, M. Yüksek, Morphological and mechanical analysis of electrospun shape memory polymer fibers, Appl. Surf. Sci. 380 (2016) 294–300.
[31] R. Erdem, I. Usta, M. Akalın, O. Atak, M. Yüksek, A. Pars, The impact of solvent type and mixing ratios of solvents on the properties of polyurethane based electrospun nanofibers, Appl. Surf. Sci. 334 (2015) 227–230.
[32] X. Lu, X. Liu, L.F. Wang, W.J. Zhang, C. Wang, Fabrication of luminescent hybrid fibres based on the encapsulation of polyoxometalate into polymer matrices, Nanotechnology 17 (2006) 3048–3053.
[33] H.Q. Yu, H.W. Song, G.H. Pan, L.B. Fan, S.W. Li, X. Bai, S.Z. Lu, H.F.J. Zhao, Preparation and luminescent properties of polymer fibers containing Y_2O_3:Eu nanoparticles by electrospinning, Nanosci. Nanotechnol. 8 (2008) 6017–6022.
[34] B. Dong, H.W. Song, H.Q. Yu, H. Zhang, R.F. Qin, X. Bai, G.H. Pan, S.Z. Lu, F. Wang, Q.L. Fan, Upconversion properties of Ln3+ doped NaYF4/polymer composite fibers prepared by electrospinning, Phys. Chem. C 112 (2008) 1435–1440.
[35] M.K. Ekmekçi, Molten Salt Synthesis and Characterization of Doped MNb_2O_6 (M = Co, Cd, Ni) Columbite Compounds (Doctoral thesis), registration number: 647103, Turkish Council of Higher Education Thesis Center, 2012.
[36] M. Sato, Y.J. Hama, Lithium insertion characteristics of $CuNb_2O_6$, J. Solid State Chem. 118 (1995) 193–198.
[37] J.M. Deitzel, J. Kleinmeyer, D. Harris, N.C. Beck Tan, The effect of processing variables on the morphology of electrospun nanofibers and textiles, Polymer 42 (2001) 261–272.
[38] E. Zussman, X. Chen, W. Ding, L. Calabri, D.A. Dikin, J.P. Quintana, R.S. Ruoff, Mechanical and structural characterization of electrospun PAN-derived carbon nanofibers, Carbon 43 (2005) 2175–2185.
[39] G.H. Dieke, Spectra and Energy Levels of Rare Earth Ions in Crystals, Interscience Publishers, New York, 1968.